Sondheimer oscillation as a signature of surface Dirac fermions

Heon-Jung Kim,[1,*] Ki-Seok Kim,[2,3] Mun Dae Kim,[4] S.-J. Lee,[5] J.-W. Han,[1] A. Ohnishi,[5] M. Kitaura,[5] M. Sasaki,[5,†] A. Kondo,[6] and K. Kindo[6]

[1]*Department of Physics, College of Natural Science, Daegu University, Gyeongbuk 712-714, Republic of Korea*
[2]*Asia Pacific Center for Theoretical Physics, POSTECH, Pohang, Gyeongbuk 790-784, Korea*
[3]*Department of Physics, POSTECH, Pohang, Gyeongbuk 790-784, Korea*
[4]*Institute of Physics and Applied Physics,Yonsei University, Seoul 120-749, Korea*
[5]*Department of Physics, Faculty of Science,Yamagata University, Kojirakawa 1-4-12 Yamagata, 990-8560, Japan*
[6]*Institute for Solid State Physics,University of Tokyo, Kashiwanoha 5-1-5, Kashiwa, Chiba 277-8581 Japan*

(Received 7 September 2011; published 30 September 2011)

Topological states of matter challenge the paradigm of symmetry breaking, characterized by gapless boundary modes and protected by the topological property of the ground state. Here, we present compelling evidence for the existence of gapless surface Dirac fermions from transport in Bi_2Te_3. We observe Sondheimer oscillation in magnetoresistance (MR). This oscillation originates from the quantization of motion due to the confinement of electrons within the surface layer. Based on Sondheimer's transport theory, we determine the thickness of the surface state from the oscillation data. In addition, we uncover the topological nature of the surface state, fitting consistently both the nonoscillatory part of MR and the Hall resistance. The side-jump contribution turns out to dominate around 1 T in Hall resistance while the Berry-curvature effect dominates in 3–4 T.

DOI: 10.1103/PhysRevB.84.125144 PACS number(s): 75.47.−m, 73.20.−r

I. INTRODUCTION

Symmetry breaking is the paradigm in not only classifying quantum states of matter but also describing phase transitions between them, where the correlation length of fluctuations between local order parameters diverges at the critical point of a continuous transition.[1,2] On the other hand, topological states of matter are classified by topological quantum numbers,[3,4] associated with gapless boundary electronic states, and are protected from the topological properties of the ground state.[5,6] Instead of a divergence in correlation length, topological phase transitions are accompanied by changes of the gapless boundary modes. One possible mechanism for this phenomenon is that the extent of the transverse wave function or the length scale of the boundary state becomes of the same order as the bulk size, causing the gapless modes in opposite boundaries to be mixed and making such boundary modes gapped.[7] In this case, this length scale for the boundary mode plays basically the same role as the correlation length for the phase transition, which is the fundamental length scale for a topological phase [Fig. 1(a)].

Recently, the semiconductor materials Bi_2Se_3 and Bi_2Te_3 have been verified to be three-dimensional topological insulators. These insulators are regarded as a novel quantum state of matter,[8–11] where gapless surface electrons are uncovered in angle-resolved photoemission spectroscopy (ARPES).[12–14] Although the surface states in these materials and the electronic structure in graphene are described by Dirac theory [Fig. 1(b)], the surface state of topological insulators is profoundly different from the electronic structure of graphene.[15] This difference originates from the absence of both the sublattice symmetry and valley degeneracy. The direction of spin is locked with that of the momentum in surface Dirac electrons.[16] This completely suppresses backscattering due to time-reversal invariant impurities, allowing a supermetallic state.[17]

In this paper we focus on MR and Hall measurements, both of which are of high importance for the fundamental understanding and practical applications of topological insulators. We observe an oscillatory behavior in MR at low magnetic fields up to 4 T. This behavior can be identified as Sondheimer oscillation,[18] where the oscillation is periodic in H. Sondheimer's transport theory,[18] combined with Dirac dispersion, enables us to determine the fundamental length scale of the topological insulator from our experimental data, which turns out to be about five atomic layers. In this respect the Sondheimer oscillation can be regarded as an inevitable result of the surface state. The nature of the surface state can be explained by the single Dirac-fermion theory. This explains not only the nonoscillatory part of MR but also the topological properties implicit in Hall resistance in a quantitative and consistent way. In particular, we show that the Hall resistance of the surface state is dominated by the side jump around 1 T and below, while the Berry-curvature contribution is dominant at higher fields.

II. EXPERIMENT

In our measurements we used defect-controlled Bi_2Te_3 single crystals. Single crystals of Bi_2Te_3 were grown by a modified Bridgman method, where Bi_2Te_3 powder is melted and crystallized in an evacuated quartz ampoule several times by slow cooling. The sample was cooled from 850 °C to 550 °C with a cooling rate of −10 K/h. Usually, as-grown Bi_2Te_3 single crystals are p doped because of the antisite defects in Bi sites.[19] In order to tune the Fermi level, we have controlled the amount of defects by adding extra Bi or Te; the doped Bi tends to increase the antisite defects, while the doped Te tends to decrease them. Based on this strategy, we have succeeded in growing a range of Bi_2Te_3 single crystals, from fully p-doped to fully n-doped regions. The carrier type is determined by thermoelectric power at room temperature and also by Hall sign measured at 4.2 K. For our experiments, we selected two p-Bi_2Te_3 samples (fully p type sample 1 and lightly p type sample 2), two insulating Bi_2Te_3 samples (TI samples, 3 and 4), and one n-Bi_2Te_3 sample (5). Samples 3 and 4 are expected to show the topological properties of the surface state well.

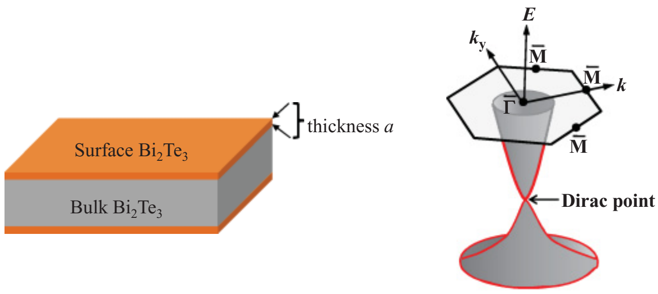

FIG. 1. (Color online) (a) The schematic diagram for Bi_2Te_3 shows the surface layer with thickness a. The surface thickness a is determined from Sondheimer oscillation in magnetoresistance. (b) The Dirac dispersion of the surface state gives rise to topologically nontrivial physical properties such as the dominant anomalous Hall effect in the Hall resistance.

Magnetoresistance (MR) and Hall-effect measurements have been carried out by a six-probe method at 4.2 K using a superconducting magnet up to 4 T and a 60 T pulse magnet at ISSP in Tokyo University up to 55 T. Here, the direction of the magnetic fields is perpendicular to the naturally cleaved plane, on which the current is applied. For the MR and Hall measurements, the six contacts are carefully made on the top surface of the sample to detect the maximum portion of the surface character and to reduce the induction noise for high-field pulse-magnet experiments. We have taken the antisymmetrized and the symmetrized parts as Hall and longitudinal resistances, respectively.

Figure 2 shows the temperature dependency of the resistivity for the p-, TI-, and n-Bi_2Te_3 single crystals. The resistivity for both the p- and n-type samples (1, 2, and 5) decreases monotonically with decreasing temperature, which is a typical metallic characteristic, while the resistivity for the TI samples (3 and 4) increases below ~180 K and then tends to saturate below 50 K. The magnitude of the resistivity for the TI-Bi_2Te_3 single crystals is 5–10 times larger than those for the p- and n-type samples. The nonmetallic nature observed for the TI samples is consistent with those reported by the Princeton group.[21]

III. SONDHEIMER OSCILLATION

ARPES has unveiled only a single Dirac-fermion band at the surface of Bi_2Te_3.[13,14] Therefore, in order to analyze our

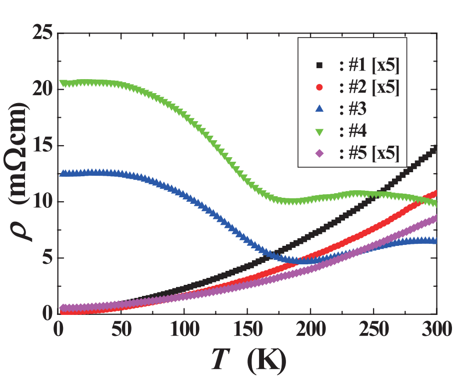

FIG. 2. (Color online) Temperature dependency of resistivity for samples 1–5.

experimental data, we introduce an electromagnetic vector potential $\vec{A}$ and a Zeeman term into the single Dirac-fermion theory. In addition, we take into account impurity scattering at the level of a Born approximation. Our theoretical analysis reveals that the orbital contribution or the effect of the vector potential on experimental data is irrelevant in the region of magnetic fields below 4 T. However, its influence on MR and Hall resistance can appear at higher magnetic fields, where Landau levels are fully developed.

Although Bi_2Te_3 is a bulk semiconducting material, the topological structure of the ground state gives rise to a surface state protected from time-reversal invariant perturbations whose extent of transverse wave function is confined within a.[8–11] Therefore, we model the surface state as a thin layer with thickness a [Fig. 1(a)], which is used in the Boltzmann equation below. This approach is essentially the same as what Sondheimer performed in metallic thin films except for the band structure, where nonrelativistic electrons are replaced with Dirac fermions in the presence of the Zeeman term. The main consequence is the quantization of motion along the direction normal to the surface, which produces an oscillatory component of MR. In our measurements at magnetic fields below 4 T, the oscillation is shown to be periodic in H.[18] This oscillation is distinguished from the Shubnikov–de Haas oscillation; due to the formation of Landau levels, it is periodic in $1/H$.

We start from the Boltzmann equation

$$-\frac{e}{\hbar}\left(\boldsymbol{E}+\frac{\bar{\boldsymbol{v}}}{c}\times\boldsymbol{H}\right)\cdot\nabla_{\boldsymbol{k}}f+\bar{\boldsymbol{v}}\cdot\nabla_{\boldsymbol{r}}f=-\frac{f-f_0}{\tau}. \qquad (1)$$

$f=f_0+f_1(\bar{\boldsymbol{v}},z)$ is a nonequilibrium distribution function with its equilibrium part f_0. The nonequilibrium part f_1 depends on the z coordinate. $\bar{\boldsymbol{v}}=\hbar\bar{\boldsymbol{k}}/m^*$ is the average velocity, where m^* is an effective mass of the surface Dirac electrons, and $\bar{\boldsymbol{k}}$ is the average momentum, which is determined later. The dispersion is given by $\epsilon_{\boldsymbol{k}}=-\mu+\sqrt{v_f^2k^2+(g^*H)^2}$ in the presence of a z-directional magnetic field H, where v_f is the Dirac velocity and the Fermi momentum is $k_f=\frac{\sqrt{\mu^2-g*H^2}}{v_f}$. μ is the chemical potential at the surface, and g^* is the Landé g factor of the surface electron. $\boldsymbol{H}=H\hat{z}$ is an applied magnetic field in the z direction and $\boldsymbol{E}=E_x\hat{x}+E_y\hat{y}$ is an electric field, where a y-directional electric field is induced. τ is the mean-free time, which measures the strength of disorder.

Following the same procedure as that in the original paper of Sondheimer,[18] we obtain

$$\rho(H,T)=\frac{\rho_0}{\kappa}\Re\phi(s), \qquad (2)$$

where $\rho(H,T)$ is the resistivity. $\rho_0=\frac{m^*}{ne^2\tau}$ is the residual resistivity with the density $n=\frac{8\pi}{3}(\frac{m^*\bar{v}}{2\pi\hbar})^3$ of surface electrons, and $\kappa=\frac{a}{l}$, where $l=\bar{v}\tau$ is the mean-free path and a is the surface thickness, determined from fitting. $\phi(s)$ results from the distribution function in the hard-wall boundary condition for the z direction, given by

$$\frac{1}{\phi(s)}=\frac{1}{s}-\frac{3}{8s^2}+\frac{3}{2s^2}\int_1^\infty du\, e^{-su}\left(\frac{1}{u^3}-\frac{1}{u^5}\right) \qquad (3)$$

after integrating over z. $s=\kappa+i\beta$, where $\beta=\frac{a}{r_c}$ with the magnetic length $r_c=\frac{m^*\bar{v}c}{eH}$, which is proportional to $1/H$. Two

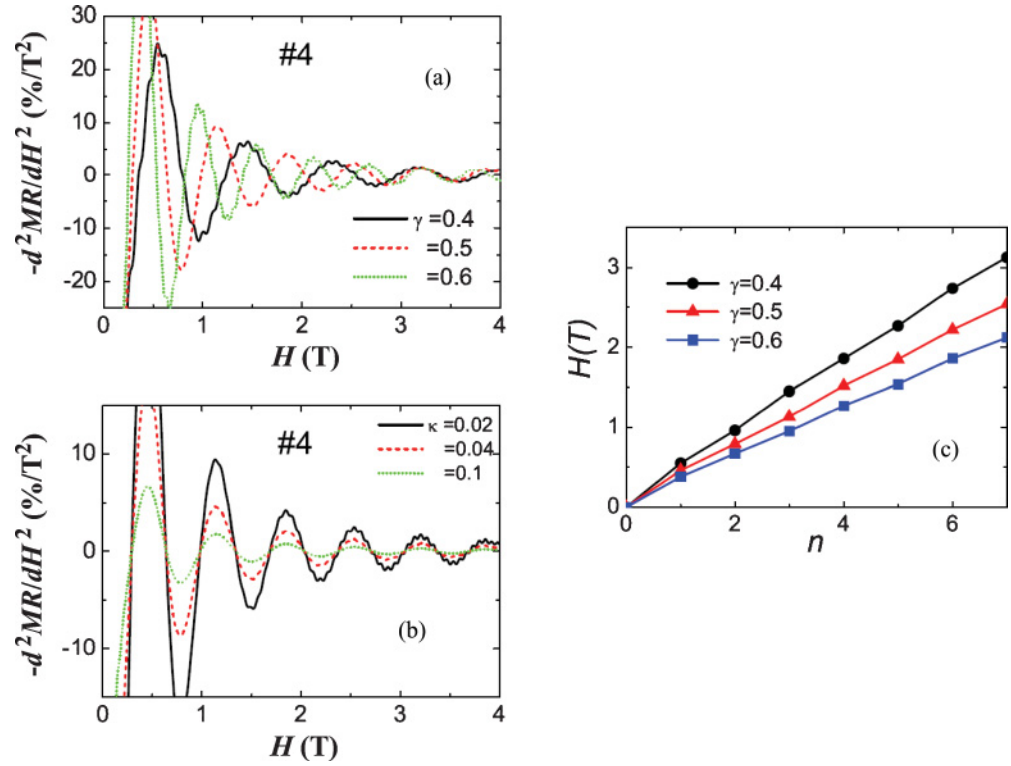

FIG. 3. (Color online) (a) Dependence of Sondheimer oscillation on the Fermi energy. $\gamma = h/H$ measures the distance of the Fermi energy from the Dirac point. Increasing γ, i.e., as the Fermi surface becomes close to the Dirac point, the period of the Sondheimer oscillation decreases. (b) Dependence of Sondheimer oscillation on the disorder strength. $\kappa = a/l$ measures the mean-free path. It does not affect the periodicity, changing the amplitude of the oscillation only. (c) Peak and dip number vs peak and dip position (magnetic fields) as a function of γ with a fixed κ.

parameters appear in this expression: $\kappa = a/l$ and $\beta = a/r_c$. This transport theory produces the H-linear periodicity. It is worth noting that the periodicity in MR depends only on β, while κ modifies the amplitude of oscillation, as shown in Fig. 3(b).

For the numerical analysis, it is important to express the β variable in terms of dimensionless parameters because the surface thickness a is determined from an appropriate choice of one parameter in β, referred to as γ, which will be discussed later. It is given by

$$\beta = \frac{1}{2}(k_f a)\frac{\hbar\omega_L}{E_F}\frac{k_f}{\bar{k}}, \quad (4)$$

where $\hbar\omega_L = \hbar\frac{eg^*H}{2m^*c}$ is the effective Zeeman energy and $E_F = \frac{k_f^2}{2m^*}$ is the Fermi energy with an effective mass m^*. $\bar{k}/k_f$ is determined from

$$\frac{\bar{k}}{k_f} = \frac{1}{t}\int_0^\infty d\epsilon \frac{\epsilon}{\sqrt{\epsilon^2+h^2}}\frac{e^{\sqrt{\epsilon^2+h^2}-\mu'/t}}{(e^{\sqrt{\epsilon^2+h^2}-\mu'/t}+1)^2}, \quad (5)$$

where we introduce several dimensionless parameters, scaled by the Fermi energy, such that an effective dispersion $\epsilon = vk/E_F$ with $v = \frac{\hbar^2 k_f}{2m^*}$, the Zeeman energy $h = \hbar\omega_L/E_F$, the chemical potential $\mu' = \mu/E_F = \sqrt{1+h^2}$, and an effective temperature $t = T/E_F$.

Based on this formulation, we fit the oscillation data of MR. First, we determine $\kappa \approx 0.02$, which characterizes the strength of the disorder for the best match of the amplitude with the Sondheimer oscillation. Although the variation of κ changes the oscillation amplitude, it does not modify the periodicity of the Sondheimer oscillation.

Our experimental data shows that the Sondheimer oscillation turns into the Shubnikov–de Haas oscillation above 3–4 T (Fig. 4). This is consistent with several recent transport measurements that show Shubnikov–de Haas oscillation beginning at around 4 T.[20–23] The appearance of the Shubnikov–de Haas oscillation is the origin for the mismatch of the oscillation amplitude.

An important point is that h also enters the nonoscillatory part of both MR and Hall resistance. Therefore, the actual value of h influences not only the periodicity of the Sondheimer oscillation but also the nonoscillatory part of both MR and Hall resistance. In order to obtain the fitting parameters reliably and consistently, we optimize not only Sondheimer oscillation but also MR and Hall resistance, simultaneously. The theoretical and experimental aspects of MR and Hall resistance will be discussed in a later section.

Combined with the longitudinal and transverse resistances, we can optimize the thickness a and the coefficient γ simultaneously, where γ is the ratio $\hbar\omega_L/E_F$ at $H = 1$ T. We found that $\gamma \approx 0.44$ and $a \approx 5$ atomic layers fit the experimental data well. It is interesting to note that the optimized γ almost coincides with the bulk value. For example, if we use bulk values of the Landé g factor and effective mass, which

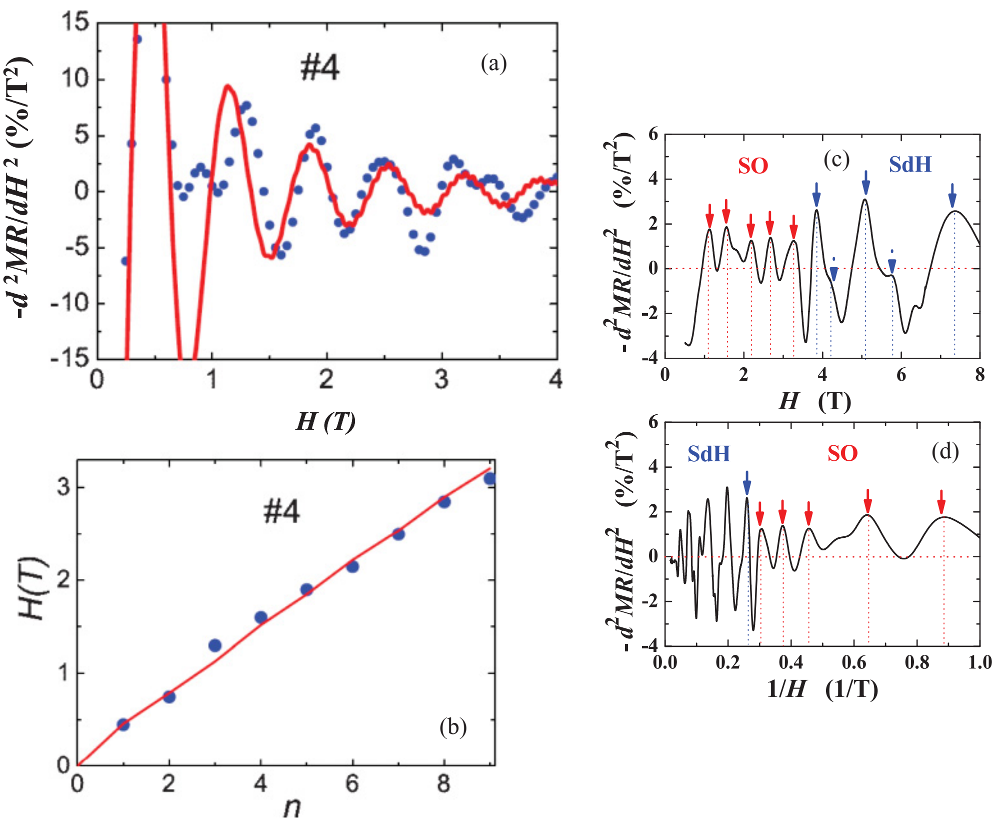

FIG. 4. (Color online) (a) The second derivative of the resistance with respect to the applied magnetic field shows oscillation with a periodicity in H, compared to the theoretical curve (red thick line) based on Sondheimer's transport theory. The experimental periodicity deviates from theoretical values around $H = 3.25$ T. (b) Peak and dip number vs peak and dip position (magnetic fields) in (a). This confirms the H linear periodicity instead of the $1/H$ periodicity. The second derivative of the magnetoresistance measured up to 55 T is plotted with respect to H (c) and $1/H$ (d). This comparison reveals that the Sondheimer oscillation exists at low magnetic fields, while the Shubnikov–de Haas oscillation with a periodicity in $1/H$ appears at high magnetic fields.

are $g^* \approx 13.7$ and $m^* \approx 0.1 m_e$ (m_e is the bare mass of an electron), we obtain $\hbar\omega_L \approx 100$ K at $H = 1$ T, giving rise to $h \approx 0.44$ with a typical bulk value for the Fermi energy $E_F \approx 230$ K. Since we cannot determine g^*, m^*, and E_F at the surface from our experiment, each value at the surface may not be the same as the bulk one. However, we would like to emphasize that the ratio γ seems to be universal in both Bi_2Te_3 and Bi_2Se_3, although both g^* and E_F in Bi_2Se_3 are almost four times larger than those in Bi_2Te_3.

Our fitting for the oscillatory part of MR, performed consistently for the nonoscillating part of both MR and Hall resistance, gives a result for the surface thickness of approximately five atomic layers. This is quite remarkable in that this value is consistent with that in molecular beam epitaxy-grown Bi_2Te_3 thin films.[24]

IV. MAGNETORESISTANCE AND HALL EFFECT

Next, we focus on the topological nature of the surface state. Strictly, the role of the single Dirac-fermion theory is not essential in Sondheimer oscillation although Dirac dispersion is utilized. It might be the case that the surface state is realized due to the good surface quality of our samples. However, we will show that the Sondheimer oscillation is a signature of surface Dirac electrons in Bi_2Te_3, verifying that the Hall resistance originates from the anomalous Hall effect of Dirac theory. In addition, we show that the side-jump contribution dominates at low magnetic fields and the Berry-curvature effect dominates at high magnetic fields.

Theoretically, the longitudinal resistance results from the transport of electrons near the Fermi surface, and can be described quasiclassically or quantum mechanically. In this case, the quasiclassical treatment based on the Boltzmann equation gives the same result as the quantum mechanical treatment based on the Kubo formula. On the other hand, there are various contributions with a topological origin in the Hall resistance, which is beyond the conventional treatment used in the Boltzmann-equation approach. The Boltzmann equation needs additional terms[25] in order to mimic the Kubo formula.[3,4]

The single Dirac-fermion theory gives an analytic expression for the longitudinal conductance[25]

$$\sigma_{xx}(H, T \to 0) = \alpha \frac{e^2}{2\pi\hbar} \frac{\sqrt{1+h^2}}{1+4h^2}, \tag{6}$$

where $\alpha \equiv \frac{4ne^2(2\pi\hbar)^3 v_f}{m^* n_I [V_I^{(0)}]^2 k_f}$ is a dimensionless parameter, which measures the strength of disorder with an impurity density n_I and an impurity potential $V_I^{(0)}$, while v_f is the Dirac-fermion velocity with the Fermi momentum k_f. We note that although both α and κ measure the strength of disorder, they differ from

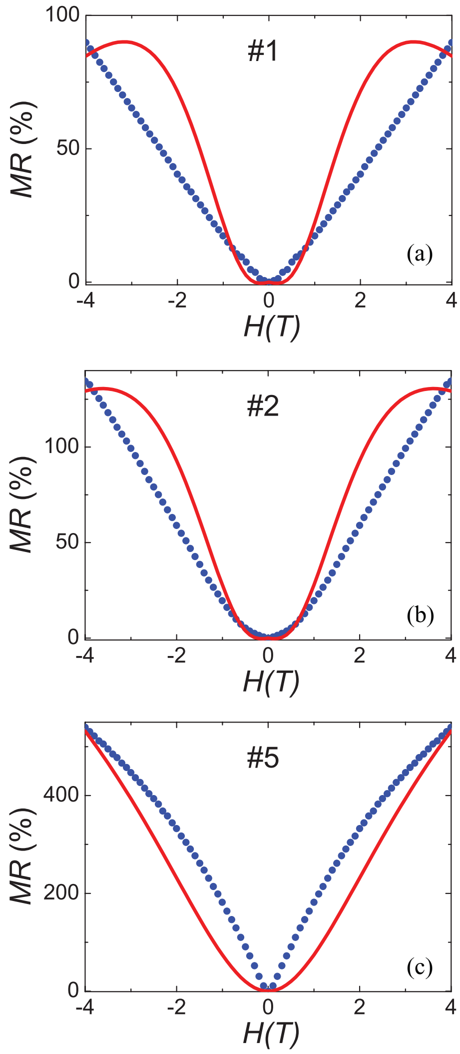

FIG. 5. (Color online) Magnetoresistance for (a) 1, (b) 2, and (c) 5, where the disorder strength is utilized as a fitting parameter, given by $\alpha \approx 0.4$, $\alpha \approx 0.5$, and $\alpha \approx 1.5$, respectively. The presence of bulk conduction channels does not allow us to describe these samples purely within the single Dirac-fermion theory.

each other due to the presence of the Fermi momentum in their relation of $\kappa \propto k_f a/\alpha$. Remember that either the Fermi momentum or the Fermi energy enters our analysis in a scaling form, not separately. h is the dimensionless magnetic field, introduced in the Sondheimer oscillation.

The same Dirac theory results in Hall conductance[25]

$$\sigma_{xy}(H,T \to 0) = \sigma_{xy}^{\mathrm{FS}}(H,T \to 0) + \sigma_{xy}^{A}(H,T \to 0),$$
$$\sigma_{xy}^{A}(H,T \to 0) = \sigma_{xy}^{B}(H,T \to 0) + \sigma_{xy}^{\mathrm{SJ}}(H,T \to 0) + \sigma_{xy}^{\mathrm{SK}}(H,T \to 0). \tag{7}$$

Hall conductance consists of two contributions. The first results from electrons near the Fermi surface, referred to as normal Hall conductance, while the second contribution comes from both the Fermi surface and Fermi sea, called anomalous Hall conductance. We use the normal Hall conductance from the Boltzman-equation approach for the Sondheimer oscillation, which is given by

$$\sigma_{xy}^{\mathrm{FS}}(H,T \to 0) = \kappa \sigma_{xx}(H,T \to 0) \frac{\Im \phi(s)}{[\Re \phi(s)]^2 + [\Im \phi(s)]^2}.$$

The anomalous Hall conductance is also composed of two contributions. The first comes purely from the topological character of the band structure, identified with the Berry-curvature term $\sigma_{xy}^{\mathrm{B}}(H,T \to 0) = -\frac{e^2}{4\pi\hbar}\frac{h}{\sqrt{1+h^2}}$, while the second originates from scattering with disorder in the presence of the spin-orbit interaction. This disorder contribution is separated into the side-jump term $\sigma_{xy}^{\mathrm{SJ}}(H,T \to 0) = -\frac{e^2}{4\pi\hbar}\frac{h}{\sqrt{1+h^2}}\{\frac{4}{1+4h^2} + \frac{3}{(1+4h^2)^2}\}$ and the skew scattering term $\sigma_{xy}^{\mathrm{SK}}(H,T \to 0) = -\eta \frac{e^2}{2\pi\hbar}\frac{h}{(1+4h^2)^2}$. It is interesting to observe that the side-jump term does not depend on the disorder strength. The dimensionless parameter $\eta \equiv \frac{[V_I^{(1)}]^3 v_f k_f}{2\pi n_I [V_I^{(0)}]^4}$ in the skew scattering term measures the disorder strength in the third order, where $V_I^{(1)}$ is a disorder strength of the third order.

Based on Eqs. (6) and (7), we obtain the longitudinal and Hall resistances as follows:

$$\rho_{xx}(H,T \to 0) = \frac{\sigma_{xx}(H,T \to 0)}{[\sigma_{xx}(H,T \to 0)]^2 + [\sigma_{xy}(H,T \to 0)]^2},$$
$$\rho_{xy}(H,T \to 0) = \frac{\sigma_{xy}(H,T \to 0)}{[\sigma_{xx}(H,T \to 0)]^2 + [\sigma_{xy}(H,T \to 0)]^2}. \tag{8}$$

It should be noted that σ_{xy} in the denominator cannot be ignored in this case because this term is comparable to σ_{xx}. Here we have two dimensionless parameters, α and η. However, the contribution from the skew scattering turns out to be negligible. Only one fitting parameter α remains for both MR and Hall resistance.

When either holes (samples 1 and 2) or electrons (sample 5) are heavily doped, MR curves greatly deviate from the single Dirac-fermion theory, as shown in Fig. 5. On the other hand, nearly insulating samples (samples 3 and 4) display reasonable matches between experiment and theory (see Fig. 6). The Hall resistance also shows deviation from the single Dirac-fermion theory for heavily doped samples (Fig. 7) but not much for nearly insulating samples (samples 3 and 4), implying that insulating samples are explained by the theory in a quantitative and consistent way. These results provide compelling evidence for topological properties of surface Dirac electrons. In particular, the dominant contribution in the Hall resistance turns out to be the side-jump mechanism at fields below 1 T and the Berry-curvature effect at higher fields. Each contribution in the Hall resistance is displayed in Fig. 8.

It is also worth noting that the curvature of the Hall resistance in sample 4 is larger than that in sample 3. According to Dirac theory with disorder, two parameters affect the shape of the Hall resistance: the disorder strength α and the parameter γ that measures the distance from the Dirac point. In Fig. 9, we show how these parameters influence the curvature of Hall resistance. Roughly speaking, to vary γ is to rescale the x axis, while to change α is to rescale the y axis. By decreasing γ, the Hall resistance becomes straighter because the anomalous

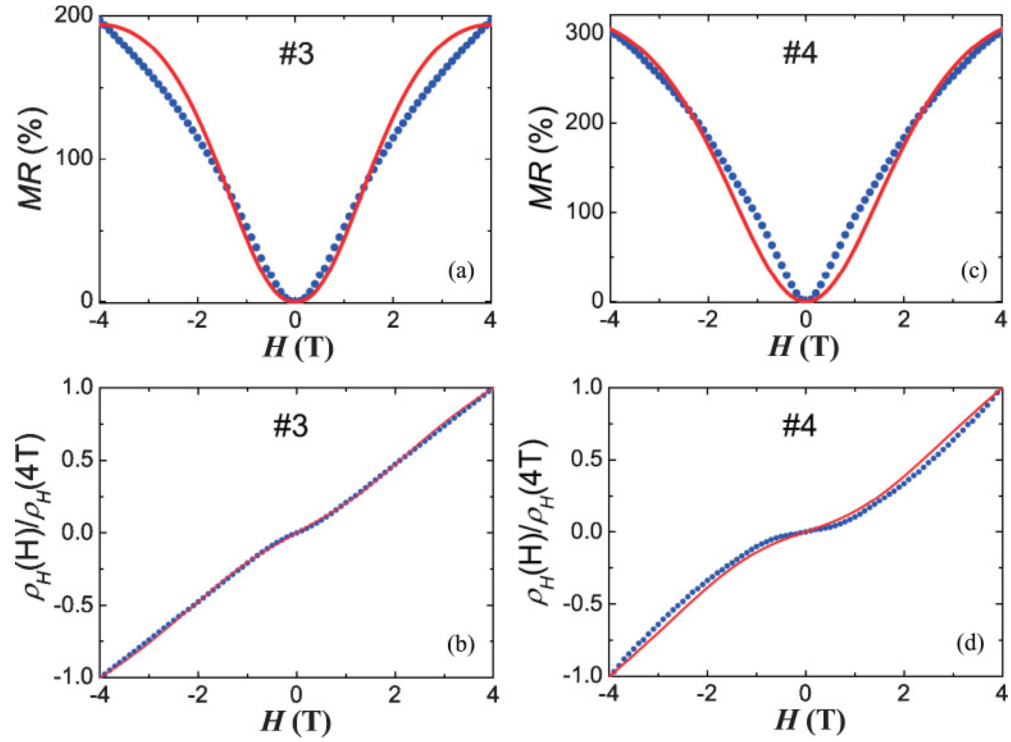

FIG. 6. (Color online) The magnetoresistance and Hall resistance of sample 3 are displayed in (a) and (b), respectively, together with theoretical curves (red thick line). The same quantities of sample 4 are presented in (c) and (d). We emphasize that the theoretical curves for Hall data are based on the parameters from our fitting of magnetoresistance data. We found that the Berry-curvature term dominates the experimental data around 3–4 T, while the side-jump mechanism works around H = 1 T, confirming the topological origin of the transport phenomena in the surface state of topological insulators.

Hall effect weakens. These results suggest that if we do not choose γ correctly, it is difficult to get a reasonable match between the experiment and theory.

V. CONTRIBUTION FROM LANDAU LEVEL

In the Sondheimer oscillation we have pointed out that the predicted oscillation amplitude does not match the experimental data because of the Shubnikov–de Haas oscillation, which occurs above 4 T. In order to confirm irrelevance of the formation of Landau levels at low magnetic fields, we take into account the vector potential for the MR and Hall resistance. This has been performed in the context of the quantum Hall effect in graphene, where the two valley contributions are simply added.[26]

The longitudinal conductance is given by[26]

$$\sigma_{xx}(H,T) = \frac{e^2 N_f \Gamma}{4\pi^2 T}\int_{-\infty}^{\infty} d\omega \frac{1}{\cosh^2\left(\frac{\omega+\mu}{2T}\right)} \frac{\Gamma}{\left(\frac{v_f^2 eH}{c}\right)^2+(2\omega\Gamma)^2}\Bigg[2\omega^2 + \frac{(\omega^2+\Delta^2+\Gamma^2)\left(\frac{v_f^2 eH}{c}\right)^2 - 2\omega^2(\omega^2-\Delta^2+\Gamma^2)\left(\frac{v_f^2 eH}{c}\right)}{(\omega^2-\Delta^2-\Gamma^2)^2+4\omega^2\Gamma^2} - \frac{\omega(\omega^2-\Delta^2+\Gamma^2)}{\Gamma}\Im\Psi\left(\frac{\Delta^2+\Gamma^2-\omega^2-2i\omega\Gamma}{2v_f^2|eH|/c}\right)\Bigg], \tag{9}$$

with $N_f = 1$ ($N_f = 2$ for graphene), where $\Delta = \hbar\omega_L$ is the Zeeman energy, Γ is the imaginary part of the electron self-energy due to disorder, and $\Psi(z)$ is the digamma function.

The Hall conductance is[26]

$$\sigma_{xy}(H,T) = \frac{e^2 N_f}{2\pi}\nu_B, \tag{10}$$

where ν_B is the filling factor, given by

$$\nu_B = \int_{-\infty}^{\infty}\frac{d\omega}{2\pi}\tanh\left(\frac{\omega+\mu}{2T}\right)\left[\frac{\Gamma}{(\omega-\Delta)^2+\Gamma^2} + (\omega \longleftrightarrow -\omega) + 2\sum_{n=1}^{\infty}\left(\frac{\Gamma}{(\omega-M_n)^2+\Gamma^2} + (\omega \longleftrightarrow -\omega)\right)\right], \tag{11}$$

where $M_n = \sqrt{\Delta^2 + 2nv_f^2|eH|/c}$ is the dispersion of surface Dirac electrons in the presence of the Landau level.

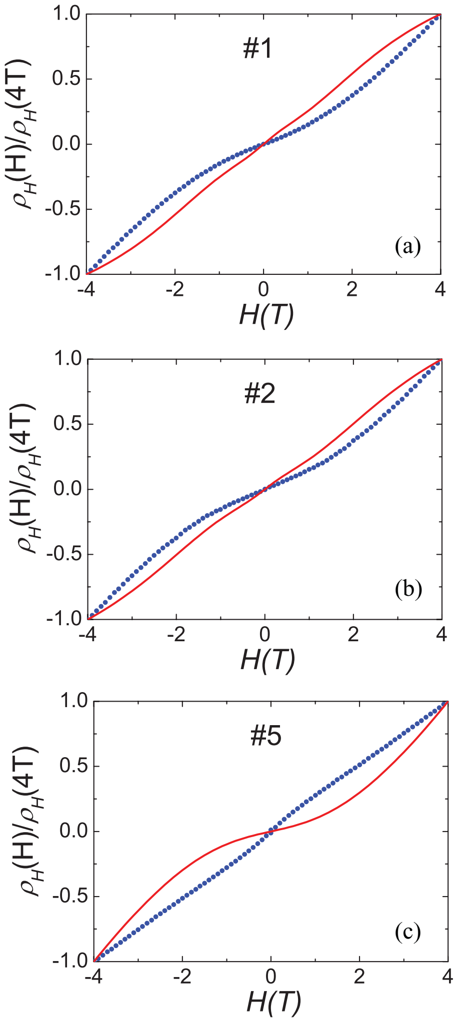

FIG. 7. (Color online) Hall resistance for (a) 1, (b) 2, and (c) 5, where the same strength of disorder is utilized as in Fig. 3, respectively. We believe that the origin of this mismatch between experiment and theory lies in the contribution from the bulk transport, which is not included in the single Dirac-fermion theory.

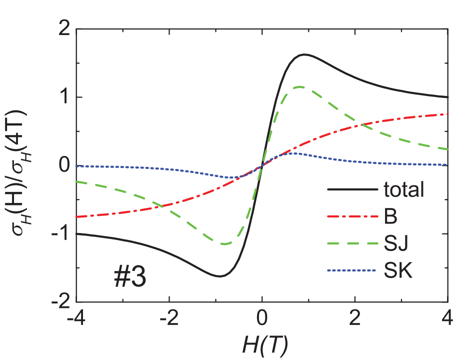

FIG. 8. (Color online) Each contribution in Hall conductance shows that the dominant term is the side-jump term in low fields and the Berry-curvature term in high fields. These curves are generated, resorting to the parameter values from sample 3, i.e., $\alpha = 0.5$ and $\gamma = 0.44$. Here, B, SJ, and SK stand for Berry curvature, side jump, and skew scattering, respectively. Total refers to the sum of all anomalous Hall contributions. The formula of each term is presented in the main text.

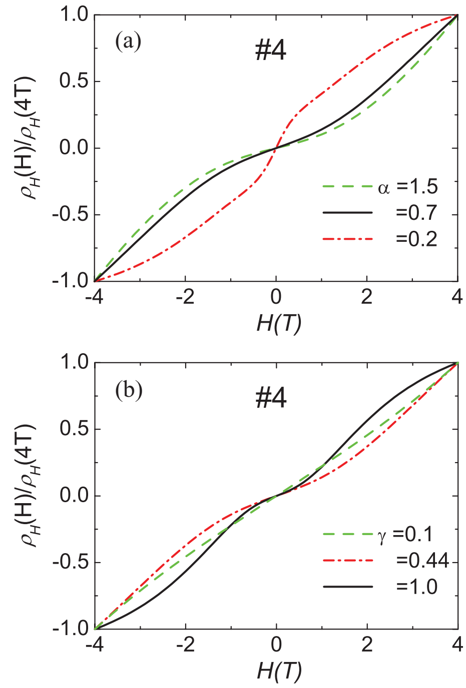

FIG. 9. (Color online) (a) Hall resistance deviates from the $\alpha = 0.7$ line with $\gamma = 0.44$, changing α. (b) Hall resistance separates from the $\gamma = 0.44$ line with $\alpha = 0.7$, varying γ. The Hall resistance of sample 4 is well fitted by $\alpha = 0.7$ and $\gamma = 0.44$.

Resorting to these expressions, we plot the Hall conductance in Fig. 10. First of all, the plateau in the Hall conductance is clearly shown. This behavior is far from that given by the experimental data. We conclude that our regime is far from being described by the quantum Hall effect. The introduction of the Zeeman term is sufficient to explain the transport data at low magnetic fields.

VI. SUMMARY AND DISCUSSION

In summary we have measured the fundamental length scale of the topological insulator, the thickness of the surface state, from the Sondheimer oscillation in magnetoresistance. This surface state is described by the single Dirac-fermion theory. The topological nature was verified by the fact that the Hall resistance results mainly from the anomalous Hall effect of

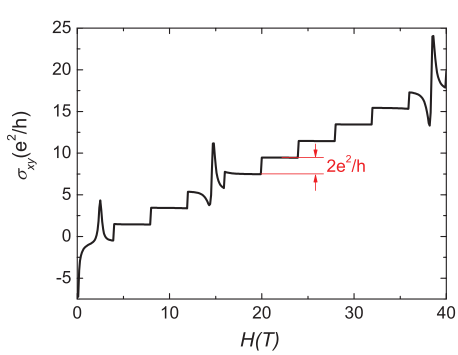

FIG. 10. (Color online) Quantized Hall conductance, expected to be relevant in high magnetic fields.

Dirac theory, which in turn is dominated by both the side-jump mechanism and the Berry-curvature effect.

The surface thickness will diverge at the critical point of a phase transition from a band insulator to a topological insulator. Such a phase transition was demonstrated in the HgTe quantum well structure when the size of the quantum well was tuned.[27,28] On the other hand, the topological phase transition has not yet been achieved in three-dimensional topological insulators. Our measurement for the surface thickness can be utilized as an important tool, revealing the mechanism of such a topological phase transition.

It is worth discussing the physical implication of the surface length scale. In our analysis, the theory of Sondheimer oscillation was worked out for a thin film within the semiclassical Boltzmann-equation approach, where electrons can move in all three directions while scattering from two hard surfaces of the thin film.[18] On the other hand, the surface states of a topological insulator may not be described by thin films but are expected to be truly two dimensional without any dispersion along the z direction.[29] This surface state is identified with a localized zero mode in the z direction and the transverse length scale in this case is the extent of the transverse wave function of the Dirac electrons.

Therefore, if the oscillation of MR in H at low magnetic fields is identified with the Sondheimer oscillation, this experimental data and our theoretical analysis suggest that Dirac electrons can have dynamics along the z direction. One possible mechanism for this z-directional dynamics is the existence of hybridization between the surface Dirac band and bulk channels. As clearly shown in our analysis of MR and Hall resistance, the two-dimensional single Dirac theory cannot explain anomalous transport in metallic samples, implying that the bulk channels may play a certain role. If the hybridization effect is introduced, the surface thickness is not just the transverse extent of the wave packet but the combination of the localized length in the z direction and an effective dynamics length, determined from the hybridization. Even though no definite answer exists for this important issue, we believe that a more elaborate quantum mechanical treatment with the hybridization effect will shed light on the possible interplay between the surface channel and bulk channels for transport in topological insulators.

We would like to point out that the Sondheimer oscillation was observed not only in insulating samples but also in metallic ones (Fig. 11). This indicates that the oscillation of MR in H is not screened by the bulk conducting channels, expected to be responsible for the oscillation in $1/H$. Actually, the Shubnikov–de Haas oscillation begins to appear at higher fields above 4 T, consistent with previous oscillation measurements.[20–23] In this respect we believe that the Sondheimer oscillation could be safely measured in a relatively low-field region.

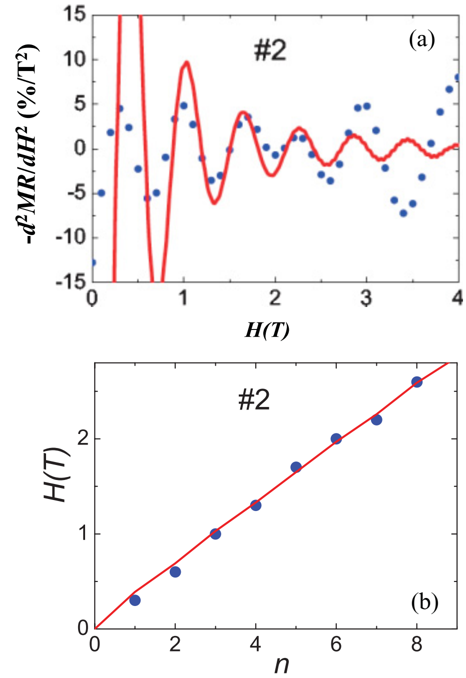

FIG. 11. (Color online) (a) Sondheimer oscillation for sample 2. The periodicity is well matched, but the oscillation amplitude deviates rather a lot due to the appearance of the Shubnikov–de Haas oscillation around 3–4 T. Sondheimer oscillations are also observed for other p- and n-doped samples, where the surface channel for conduction coexists with the bulk conduction. (b) Peak and dip number vs peak and dip position (magnetic fields) in (a). Data points are located on a straight line, confirming the H linear periodicity instead of the $1/H$ periodicity.

It is also an important issue to determine whether the Shubnikov–de Haas oscillation originates from surface states or from bulk states. One way will be to compare Shubnikov–de Haas oscillations of insulating samples with those of metallic ones. We expect that both the amplitude and period in $1/H$ for the Shubnikov–de Haas oscillation will vary, depending on the concentration of impurities, which allows us to control bulk conduction through localization while the conduction of surface Dirac fermions will not be affected so much due to topological protection.

ACKNOWLEDGMENTS

This research is supported by Basic Science Research Program through the National Research Foundation of Korea (NRF) funded by the Ministry of Education, Science, and Technology (Grant No. 2011-0025771). K.-S.K. is supported by the National Research Foundation of Korea (NRF) grant funded by the Korea government (MEST) (Grant No. 2011-0074542).

*hjkim76@daegu.ac.kr
†sasaki@sci.kj.yamagata-u.ac.jp

[1] V. L. Ginzburg, Rev. Mod. Phys. **76**, 981 (2004).
[2] Y. Nambu, Rev. Mod. Phys. **81**, 1015 (2009).
[3] N. Nagaosa, J. Sinova, S. Onoda, A. H. MacDonald, and N. P. Ong, Rev. Mod. Phys. **82**, 1539 (2010).
[4] D. Xiao, M.-C. Chang, and Q. Niu, Rev. Mod. Phys. **82**, 1959 (2010).

[5]M. Z. Hasan and C. L. Kane, Rev. Mod. Phys. **82**, 3045 (2010).
[6]C. Nayak, S. H. Simon, A. Stern, M. Freedman, and S. D. Sarma, Rev. Mod. Phys. **80**, 1083 (2008).
[7]R. Shindou, R. Nakai, and S. Murakam, New J. Phys. **12**, 065008 (2010).
[8]L. Fu, C. L. Kane, and E. J. Mele, Phys. Rev. Lett. **98**, 106803 (2007).
[9]J. E. Moore and L. Balents, Phys. Rev. B **75**, 121306 (2007).
[10]R. Roy, Phys. Rev. B **79**, 195322 (2009).
[11]R. Roy, Phys. Rev. B **79**, 195321 (2009).
[12]D. Hsieh, D. Qian, L. Wray, Y. Xia, Y. S. Hor, R. J. Cava, and M. Z. Hasan, Nature (London) **452**, 970 (2008).
[13]D. Hsieh, Y. Xia, L. Wray, D. Qian, A. Pal, J. H. Dil, J. Osterwalder, F. Meier, G. Bihlmayer, C. L. Kane, Y. S. Hor, R. J. Cava, and M. Z. Hasan, Science **323**, 919 (2009).
[14]Y. L. Chen, J. G. Analytis, J.-H. Chu, Z. K. Liu, S.-K. Mo, X. L. Qi, H. J. Zhang, D. H. Lu, X. Dai, Z. Fang, S. C. Zhang, I. R. Fisher, Z. Hussain, and Z.-X. Shen, Science **10**, 178 (2009).
[15]A. H. Castro Neto, F. Guinea, N. M. R. Peres, K. S. Novoselov, and A. K. Geim, Rev. Mod. Phys. **81**, 109 (2009).
[16]D. Hsieh, Y. Xia, D. Qian, L. Wray, J. H. Dil, F. Meier, J. Osterwalder, L. Patthey, J. G. Checkelsky, N. P. Ong, A. V. Fedorov, H. Lin, A. Bansil, D. Grauer, Y. S. Hor, R. J. Cava, and M. Z. Hasan, Nature (London) **460**, 1101 (2009).
[17]K. Nomura, M. Koshino, and S. Ryu, Phys. Rev. Lett. **99**, 146806 (2007).
[18]E. H. Sondheimer, Phys. Rev. **80**, 401 (1950).
[19]Y. S. Hor, A. Richardella, P. Roushan, Y. Xia, J. G. Checkelsky, A. Yazdani, M. Z. Hasan, N. P. Ong, and R. J. Cava, Phys. Rev. B **79**, 195208 (2009).
[20]A. A. Taskin and Y. Ando, Phys. Rev. B **80**, 085303 (2009).
[21]D. Qu, Y. S. Hor, Jun Xiong, R. J. Cava, and N. P. Ong, Science **329**, 821 (2010).
[22]J. G. Analytis, R. D. McDonald, S. C. Riggs, J.-H. Chu, G. S. Boebinger, and I. R. Fisher, Nat. Phys. **6**, 960 (2010).
[23]Z. Ren, A. A. Taskin, Satoshi Sasaki, Kouji Segawa, and Yoichi Ando, Phys. Rev. B **82**, 241306 (2010).
[24]C.-L. Song, e-print arXiv:1007.0809.
[25]N. A. Sinitsyn, A. H. MacDonald, T. Jungwirth, V. K. Dugaev, and Jairo Sinova, Phys. Rev. B **75**, 045315 (2007).
[26]E. V. Gorbar, V. P. Gusynin, V. A. Miransky, and I. A. Shovkovy, Phys. Rev. B **66**, 045108 (2002).
[27]B. A. Bernevig, T. L. Hughes, and S. C. Zhang, Science **15**, 1757 (2006).
[28]M. Konig, S. Wiedmann, C. Brune, A. Roth, H. Buhmann, L. W. Molenkamp, X.-L. Qi, and S.-C. Zhang, Science **2**, 766 (2007).
[29]We would like to thank J. K. Jain for clarifying the difference between the surface state in a topological insulator and that in a thin film.